ICAS 2016
30th Congress of the International Council of the Aeronautical Sciences
DCC, Daejeon, Korea ; September 25-30, 2016

KAI SURION HELICOPTER FULL-SCALE AIR INTAKE TESTING AT CIRA ICING WIND TUNNEL

A.C. de Bruin [*], G. Fatigati [**], H.B. Shin [***]
[*]NLR, [**]CIRA, [***]KAI

Keywords: *Icing Tests, Icing Wind Tunnel, anti-icing system*

Abstract

In order to check the anti-icing system for the air intakes of the KAI Surion helicopter, dedicated anti-icing qualification tests were made in the CIRA icing wind tunnel. The paper presents the design, manufacturing and testing of two full scale air intake models. One model was used for aerodynamic verification tests and the other model was used for the actual anti-icing tests and therefore equipped with an electro-thermal anti-icing system. This paper gives a description of the models, their instrumentation, the wind tunnel, the tests and some characteristic test results.

1 Introduction

The Korean Utility Helicopter ("KUH"), Surion, is developed by the Republic of Korea Government ("ROKG") and is providing troop and cargo transport, search & rescue, air assault operation, command & control, and multi-role missions. To enable all-weather operations, the air intakes of the Surion helicopter are protected by an electro-thermal anti-icing system. In support of the military certification process, Korea Aerospace Industries Co. LTD, KAI, contracted NLR (the Netherlands Aerospace Centre), to integrate full scale air intakes into a wind tunnel model and to perform tests at icing conditions in the CIRA (Centro Italiano Ricerche Aerospaziali) Icing Wind Tunnel.

The present paper gives a description of the models, their instrumentation, the icing wind tunnel, the test methodology and a summary of the results obtained in the CIRA icing wind tunnel that finished at the beginning of 2012.

2 The intake models

In the intake models only part of the helicopter geometry needs to be represented. KAI provided to NLR a full-scale air intake, equipped with an electro-thermal anti-icing system and a controller (Fig. 1) and a second "aerodynamic" intake without installed heating system (Fig. 2).

Fig. 1: Thermal intake model in IWT

Fig. 2: Aerodynamic intake model in IWT

NLR adapted and integrated these full scale parts into a wind tunnel model mock-up, as shown in Fig. 3. The core of the mock-up is a stainless steel frame on which the different parts are mounted (the yellow part in Fig. 3).

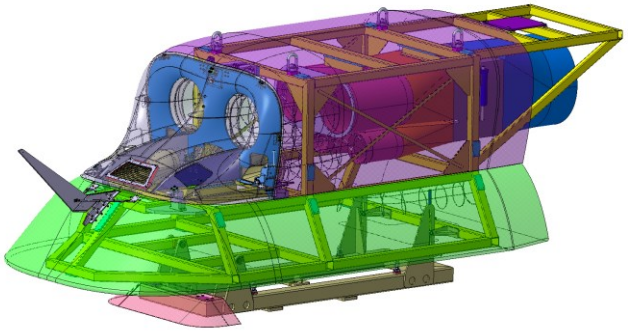

Fig. 3: The wind tunnel model mock-up

The following model parts are distinguished:

- The bottom streamlining part of the mock-up (the green part in Fig. 3) represents the upper part of the helicopter cockpit and fuselage. This part was designed and manufactured by NLR.
- An "aerodynamic intake" (AI) provided by KAI, and subsequently equipped with pressure taps by NLR (see Fig. 4 for the pressure hole positions), in order to measure the pressure distribution in different model settings (alpha and beta) and test conditions;
- A "thermal intake" (TI) provided by KAI, equipped with an embedded electro-thermal Ice Protection System including thermal controls. On the intake lips, just outside the protected area, NLR installed a strip with an Additional Heater Mat (AHM), the copper colored strips around the inlets shown in Fig. 5, for optional application during the tests, if needed. NLR also installed 27 temperature sensors on top of the heater mats (see Fig. 5).
- An engine cowling head (purple part in Fig. 3, designed and manufactured by NLR) to reproduce the engine cowl geometry of the Surion helicopter.
- A cable cutting device, optionally mounted on the bottom streamlining part
- screens for optional testing of a passive IPS to be mounted on the aerodynamic intake (see Fig. 6, screens provided by KAI);
- A central mass flow controller designed and manufactured by NLR together with its interface with the intake ducts and to the Engine Flow Simulator (EFS) system of the wind tunnel.

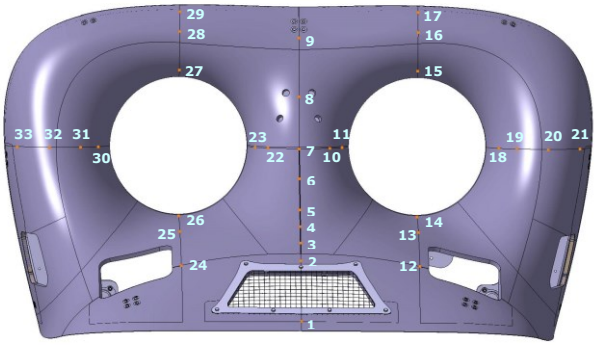

Fig. 4: Pressure hole positions on AI model

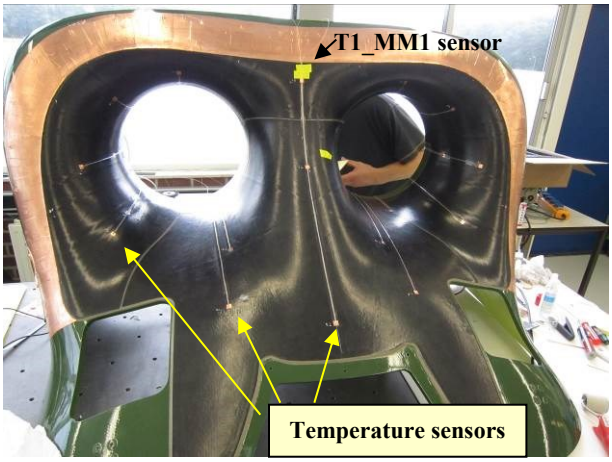

Fig. 5: Temperature sensors installed by NLR on top of the heater mat of the TI model

Fig. 6: Model with passive IPS screens in IWT

The Surion intake model has 5 intake ducts. The two engine intakes and the two nacelle cooling air scoops were connected with flexible hoses to the central flow control unit having a remotely controlled flap type valve to control the mass-flow partition between the engine intakes and the engine cooling intakes (see Fig 7). The central mass flow control unit, having a single duct exit, was connected to the tunnel suction system. The fifth central air scoop, meant for the Electronics Cooling System (ECS), was passively discharged into the tunnel flow at the lee-side of the model. Fig. 8 shows the intake suction channels, the mass flow control flap lever and the rake position.

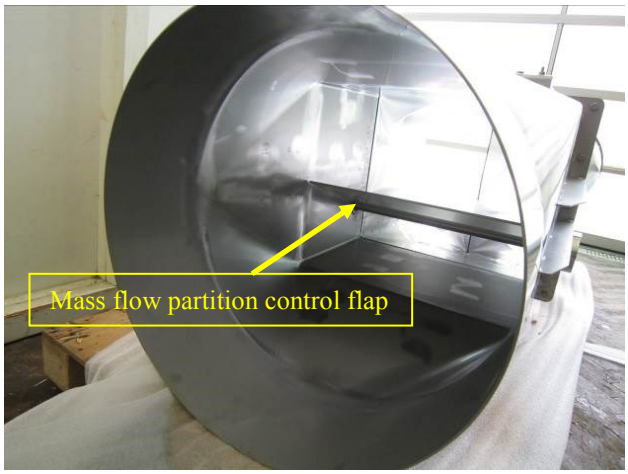

Fig. 7: Mass flow partition control flap in the collective suction duct, seen from the aft-side

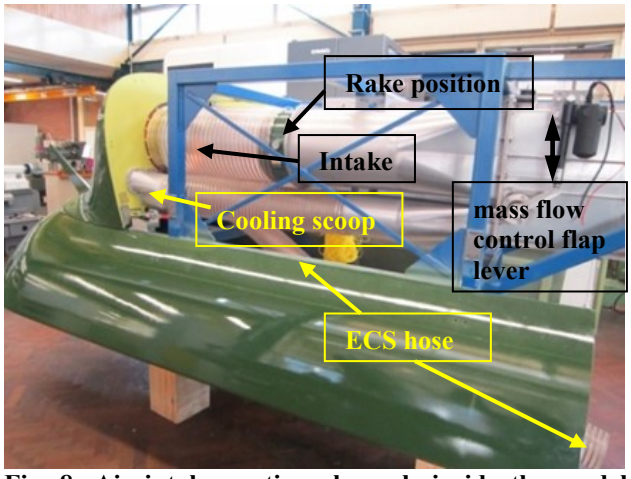

Fig. 8: Air intake suction channels inside the model mock-up (engine cowling removed).

The inlet mass flow measuring system, consisting of static pressure ports and a total pressure rake with 7 tubes mounted directly behind both the AI and the TI inlet (see Fig. 8), is shown in Fig. 9. It should be noted that during icing tests the pitot rake is turned backwards to prevent accretion in the total pressure tubes. Under these conditions rather static instead of total pressures are measured with the rake.

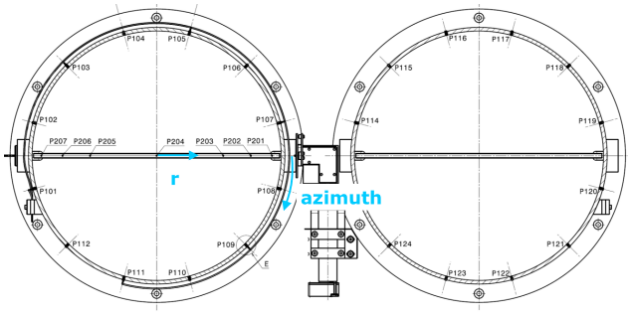

Fig. 9: Total pressure rake (7 probes) in RH inlet and 12 static pressure ports around each inlet

3 The CIRA icing wind tunnel

Inaugurated in September 2002, the CIRA Icing Wind Tunnel (IWT) owns world-wide unique testing capabilities for ice accretion and ice protection systems performance assessment, in accordance with acknowledged test techniques, best-practices and measurement methods accepted by airworthiness authorities. The CIRA IWT, situated in Capua in Italy, is a large and advanced icing facility specialized in ice protection system testing and experimental research on ice formation (see Fig. 10). It allows real altitude air density/pressure, temperature, velocity and cloud condition simulation in a controlled and repeatable environment. It is also provided with a suction system to control the flow through the intakes.

Fig. 10: CIRA Icing Wind Tunnel

The IWT has a closed loop refrigerated and pressurized circuit, for aerodynamic and icing tests. It has three interchangeable test sections and one Open Jet configuration. The configuration used for the KAI tests was the so-called Additional Test Section having width, height and length dimensions of 3.60x2.35x8.50 m^3, for which the maximum Mach number is 0.25. The test section is surrounded by a plenum chamber and can have either closed or slotted walls. During the KAI tests, the closed wall configuration was used.

Airflow refrigeration is obtained via a twin row heat exchanger. The minimum achievable static temperature in the test section is –32 °C. An air evacuation/pressurization system allows static pressure being regulated between 39,000 Pa, corresponding to an altitude of about 7,000 m, and 145,000 Pa, for high Reynolds number aerodynamic tests. The entire tunnel outer shell is thermally insulated and airtight.

For simulating icing conditions, the cloud generation is carried out by a Spray Bar System, able to generate water droplets with specific Median Volumetric Diameters (MVD) and Liquid Water Content (LWC), covering the overall envelope prescribed by FAR 25/29 Appendix C for both continuous and intermittent cloud conditions. Furthermore, the system is capable to generate Super-Cooled Large Droplets, within the range of freezing drizzle conditions.

The cloud is generated by the spray nozzles of the Spray Bar System (SBS), consisting of 20 aerodynamically shaped stainless steel and horizontal placed bars (details shown in Fig. 11), which are mounted on a frame, positioned in the settling chamber and are properly fed by two separate supply lines, one for pressurized de-mineralized water and one for air. Each bar can host up to 50 nozzles. Depending on required MVD and LWC to be generated by the SBS system, the corresponding air and water supply pressures are known from previous calibration (see e.g. [5]) and they are reached by proper control of the air and water supply valves for each bar. The system allows also to set different nozzle patterns (map of the position on which nozzles are mounted and activated), so as to match the requested LWC and optimize the cloud uniformity.

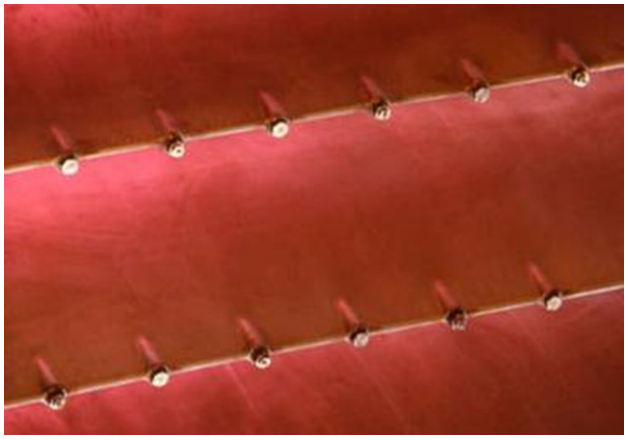

Fig. 11: Close-up of a few bar trailing edges equipped with spraying nozzles

The air is directly injected into the settling chamber whilst the water pipe to the nozzle is equipped with a remotely controlled solenoid valve that is opened only when the command SPRAY ON is given by the operator. The two fluids mix right before the spraying nozzle in a small premixing chamber. Afterwards the bi-phase fluid, passing through the spray nozzle, generates the droplets of the specific MVD and LWC and releases them into the flow inside the settling chamber. It should be noted that in reality the droplets are created with a certain spectrum of the droplet diameter distribution. For a given SBS operational setting, the LWC scales about inverse proportional with the wind tunnel speed.

Fig. 12 shows the maximum and minimum attainable LWC as function of the MVD for different wind tunnel speeds. As can be seen the SBS largely covers The FAR 25/29 Appendix C LWC-MVD envelopes for Intermittent Maximum Icing (IMI) and Continuous Maximum Icing (CMI) conditions. The droplet cloud, generated in the settling chamber, is drawn into the test section by the flow. The tunnel contraction between the settling chamber and the test section is 18 m long (longer than in a standard aerodynamic tunnel) to allow enough residence time for the droplets to accommodate

(accelerate) to the flow, their natural drop speed and let them thermally stabilize with the flow.

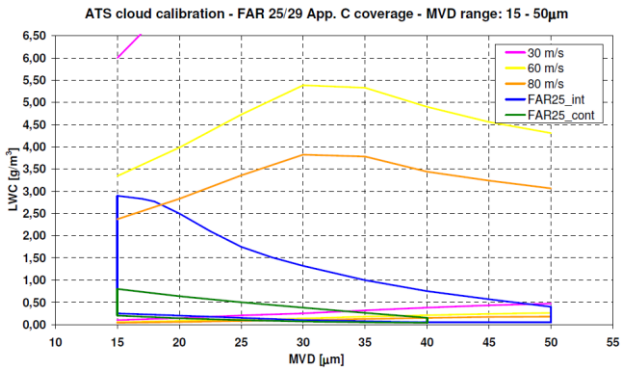

Fig.12: SBS envelope (different tunnel speeds) against FAR25/29 Appendix C

The total mass flow through the engine and cooling ducts is controlled through and measured by the Engine Flow Simulator (EFS) system (see Fig. 13). The mass flow rate is measured within 1 % accuracy and the air is returned into the tunnel circuit far downstream of the test section. Two systems are available, a large mass flow system (EFS#1) and a smaller mass flow system (EFS#2).

Fig 13: Fans and pipes of the EFS system.

An introduction to ice wind tunnel testing can be found in [1] and [2]. Whereas a description of the IWT features is given in [4].

4 The tests in CIRA IWT

Prior to the tests a dedicated test matrix was defined by KAI with input from CIRA and NLR. Some of the selected icing test conditions required additional dedicated calibrations of the SBS, prior and after the actual icing tests.

The actual test campaign started with a series of aerodynamic reference tests with the Aerodynamic Intake (AI) model, during which the pressure distributions on the intake lips and inside the engine air intake ducts were measured under various engine mass flow and model pitch and side slip flow conditions. The maximum attainable speed of the wind tunnel with the intake model installed turned out to be 65 m/s.

The stability and uniformity of the air flow in the air intake ducts was monitored at the rake position from total and static pressures (see Fig. 9). An example of time-averaged measured and calculated pressure coefficients at all 33 pressure ports of the inlet (see Fig. 4) is shown in Fig. 14 for the test case α=-5, β=-2 deg.

Fig. 15 shows an example of the mass flow measured with the EFS#1 system and mass flows estimated from the static pressure distribution in the rake planes downstream of the intakes and from one pitot static tube placed in the suction system far downstream of the model. Note that the total measurement period is almost one hour. EFS#1 displays weak long period (about 250 s) fluctuations in the mass-flow. Related, but much larger mass flow oscillations (correlated with EFS mass flow variation) are found in the rake static pressures and the pitot tube mass flow estimates.

These large fluctuations are caused by flow separations in the ducts, causing unreliable mass flow estimates for the intakes. When the tunnel speed is increased, the total mass flow through the EFS system is preserved by the EFS controller. Also the difference between the rake mass flow estimate (mass flow through the engine ducts) and the pitot tube mass flow estimate (total mass flow estimate) decreases. This indicates that the mass flow through the cooling ducts decreases.

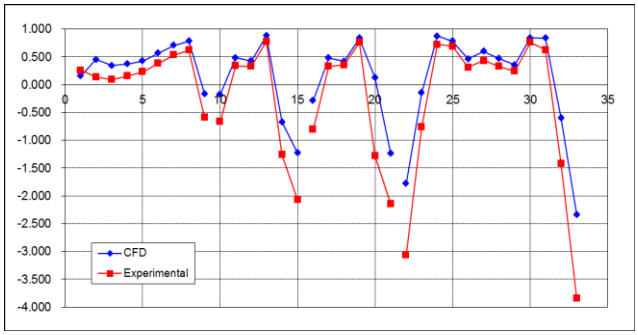

Fig. 14: Comparison of measured and calculated C_p values in the inlet α=-5, β=-2 deg. Note that sensor # is along horizontal axis (see Fig. 4 for actual positions).

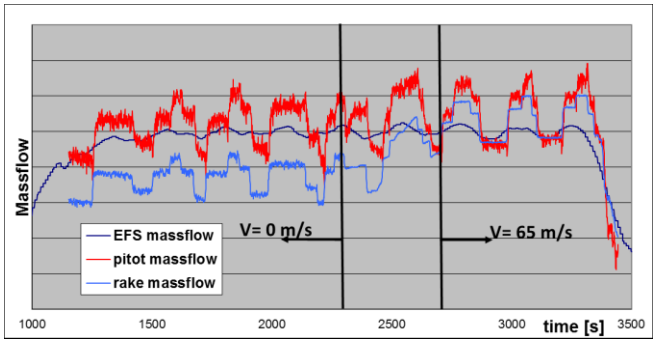

Fig. 15: Comparison of mass flow measured with EFS#1 system and mass flow estimates from rake section and pitot tube.

Various mass flow partition control vane settings were tried, with and without an extra installed wooden obstruction block mounted onto the top wall of the mass flow partition box. Due to internal pressure losses in intake and mass flow partition box and the reduced air density at simulated altitude, all tests had to be made with the large capacity EFS#1 system. It appeared difficult to obtain stable mass flow conditions with the EFS#1 system coupled to this particular model. This also made it difficult to control the proper mass flow partition between main engine intakes and cooling ducts. A test with wool tufts near and in the cooling ducts, revealed that during tunnel wind-on conditions effectively almost no air went through the cooling scoops.

After it was found that complete internal blocking of the cooling ducts (icing test ID10bis) did not have an appreciable effect on ice formation, it was decided to apply zero angle setting of the control vane and keep the wooden obstruction block in the central flow control unit during all further testing.

With the Thermal Intake (TI) model with its electro-thermal anti-icing system, 20 tests were carried out for carefully selected DEF-STAN flight and cloud conditions. In total 35 conditions were tested, including heater-off, a ground idle and a flight idle descent and some FAR conditions, not discussed here. The DEF-STAN conditions included both Intermittent Maximum Icing (IMI) and Continuous Maximum Icing (CMI) conditions, as shown in Fig. 16 and 17. In these figures FAR conditions for 0, -10, -20 and -30 °C are shown for reference only.

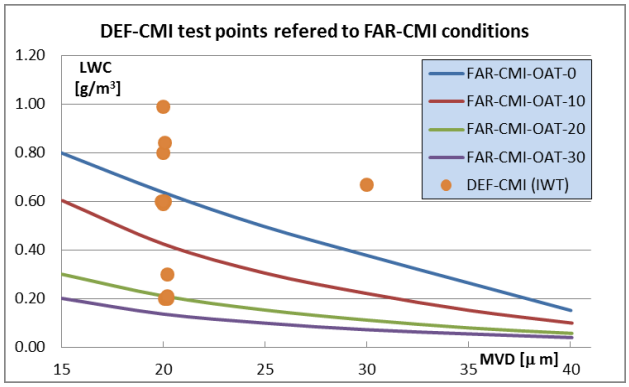

Fig. 16: Tested Continuous Maximum Icing conditions (DEF-CMI), referred to FAR-CMI.

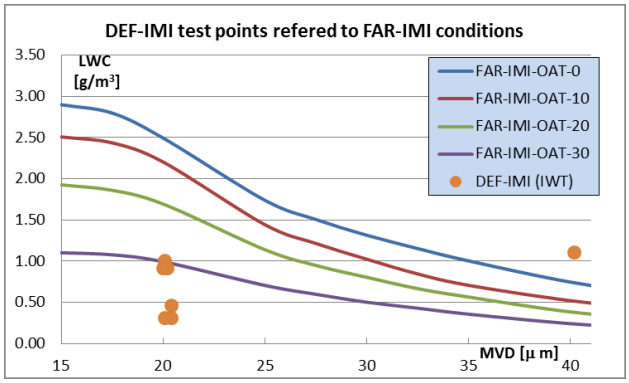

Fig. 17: Tested Intermittent Maximum Icing conditions (DEF-IMI), referred to FAR-IMI.

The following wide range of test conditions was covered: LWC from 0.14 to 1.74 g/m^3, MVD from 20 to 40 µm, exposure time from 74 to 1800 seconds, air temperature from -30 to +5 °C, simulated altitude from 0 to 4300 m, air

velocity from 20 to 65 m/s (the maximum attainable tunnel speed with the intake model installed). The model angle of attack/side slip was taken as -5/-2 deg. for 4300 m altitude tests, -1/-1 deg. for 1500 m tests and -5/0 deg. for the 0 m altitude tests. During all tests, except ID22 and ID35, the anti-icing system was activated prior to spray-on. So no delayed actuation was tested.The alternative heater mat (AHM) was only activated during ID34 and ID35 test. A summary of the DEF-CMI and DEF-IMI test conditions is given in Table 1.

5 Discussion of anti-icing test results

The effect of the anti-icing system was monitored by means of surface temperature sensors. A sophisticated infrared camera was used for real-time recording of the complete air intake surface thermal characteristics (Fig. 18).

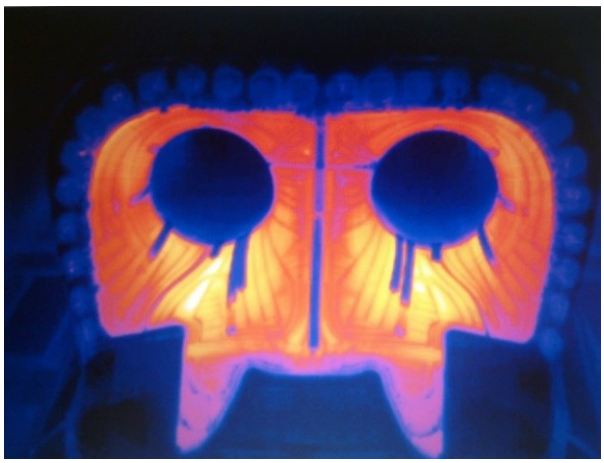

Fig. 18: Example of real-time infra-red image of air intake with anti-icing system on.

Each test run starts with a tunnel stabilization phase, for establishing the proper pressure, temperature, wind tunnel speed and total inlet mass flow. When stable conditions are reached, the anti-icing system is switched on. When the spray bars are switched on, a short period, lasting approximately 20 to 40 seconds, is needed to stabilize the spray bar system after which the tests are continued for the requested exposure time. In general, during this period the anti-icing system needs to operate at full power, but the model cools down slowly until a stable situation is reached. At the end of the test run both the spray and heating system are switched off.

Examples of a time histories of measured surface temperatures, for DEF-CMI cases ID15 and ID16, with ambient air temperature conditions of -10 and -30 °C, are shown in Fig. 19 and Fig. 20.

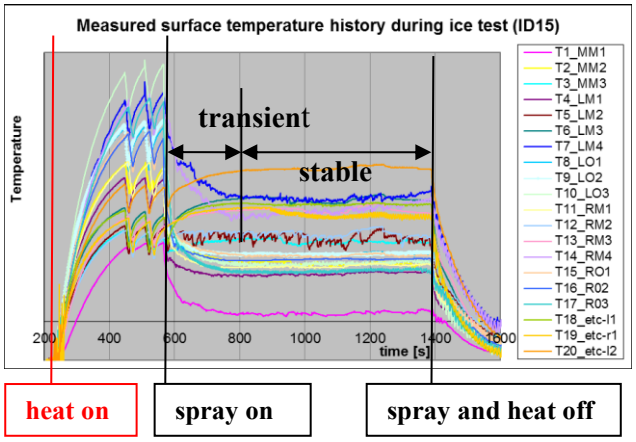

Fig. 19: Example of measured surface temperatures during DEF-CMI ice test ID15 (LWC=0.60g/m^3, MVD=19.9µm, T=-10 °C, exposure time 782 s).

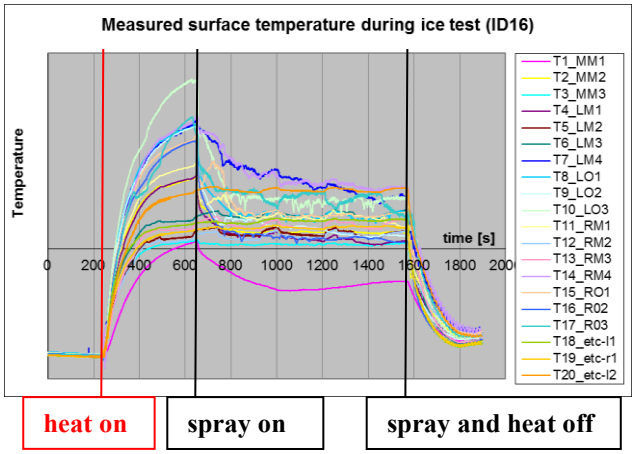

Fig. 20: Example of measured surface temperatures during DEF-CMI ice test ID16 (LWC=0.21g/m^3, MVD=20.2µm, T= -29.9 °C, exposure time 782 s).

In both cases there is a sharp rise of surface temperature soon after the anti-icing system has been switched on. The preparation phase of the test consists in warming up the surface to a stable temperature. To keep surface

temperatures below a safe maximum allowed value, the anti-icing system controller demands intermittent on/off of the heating elements for the T= -10.0 °C case (ID15) but not for the T= -29.9 °C case (ID16). When a more or less (intermittent) stable surface temperature distribution is reached, the spray bars are switched on and the model cools down. For the ID15 case all measured surface temperatures on the intake surface stabelize above zero deg., indicating a low risk for ice accretion on the protected area. For the ID16 case only the temperature for the T1_MM1 sensor (its position is shown in Fig. 5) comes well below zero.

Fig. 21 shows the temperature history for a DEF-IMI test case (ID18) with an ambient air temperature of -30 °C. This time, when the anti-icing system is activated it takes about 700 seconds until stable surface temperatures are reached and these remain below the maximum allowed surface temperature, so no intermittent operation of the anti-icing system is needed. In this case after switching on the spray bars, the surface temperature drops fast. No stable temperature condition is reached within the requested IMI exposure time of 117 s. During spray bar on, some surface temperatures now drop below zero, indicating that in this more severe IMI case there is a larger risk of ice accretion than for the CMI case of Fig. 20. Yet, due to the relatively short exposure time, the ice accretion remains acceptable.

Directly after each test, the tunnel was brought to atmospheric pressure and entered (see Fig. 22) to photograph and measure any ice accretion on the model. A special device was placed on the nose of the model, to support and slide pre-heated (properly contoured) copper plates against the inlet surface, such as to create cross-sections through the ice for subsequent ice contour measurements (see Fig. 23).

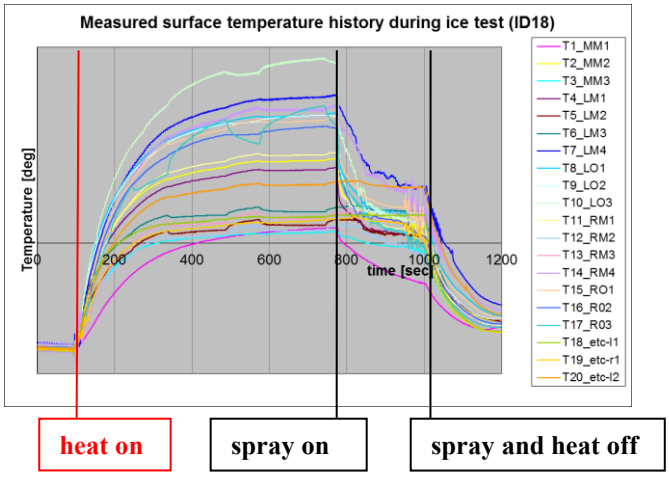

Fig. 21 Example of measured surface temperatures during DEF-IMI ice test ID18 (LWC=0.31g/m^3, MVD=20.1μm, T=-30.0 °C, exposure time= 117 s).

One test (ID22) was performed with anti-icing systems off during 1200 s (20 minutes). In this case ice accretion occurred not only on the intake lips, but also inside the ducts, especially at the upper side of the ducts (see Fig. 24). The flow stagnation region with low ice accretion (due to the local surface heating generated by the conversion of the droplet kinetic energy into heat) is clearly visible (the red marked areas in Fig. 24).

All test results were analyzed in detail by KAI in support of the anti-icing system qualification process. As part of that work ice simulation computations have been made by KAI and have been reported in [3].

Fig. 22: Entering the CIRA IWT directly after ID10 icing test.

Fig. 23: Ice accretion measurements, directly after the ice test

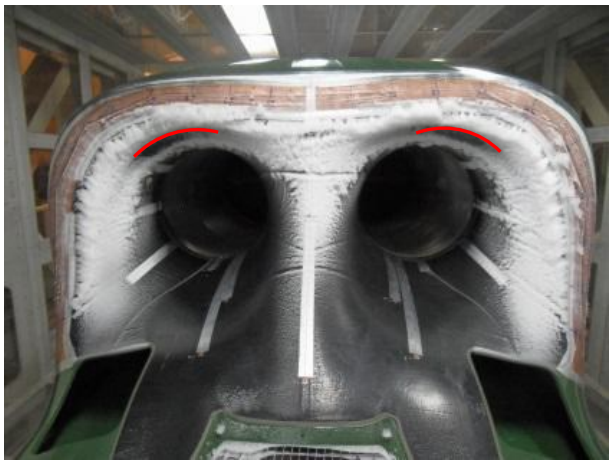

Fig. 24: Ice accretion after a test with anti-icing systems switched off, test ID22 (LWC=0.60 g/m3, MVD= 20 µm, T=-10.0 °C, exposure time= 1200 s)

5 Conclusions

A full scale model for the air intakes of the Korean Utility Helicopter (KUH), Surion, with installed anti-icing system has been prepared by NLR for anti-icing qualification tests by KAI in the CIRA Icing Wind Tunnel.

With the specific model and wind tunnel EFS#1 mass flow controller combination, it proved difficult to accurately control the mass flow through the cooling ducts. Based on tuft visualization tests the mass flow through the cooling ducts was very low during the tests.

A test program of 33 icing test conditions was successfully completed. The test program included tests at sea level, cruise (1500m) and high altitude (4300m) for a variety of Intermittent Maximum Icing (IMI) and Continuous Maximum Icing (CMI) conditions.

The anti-icing system was qualified for certification flight testing. Artificial and natural icing certification flight tests have recently been made with NLR assistance. These flight tests were successfully completed in March 2016.

Contact Author Email Address

mailto: anton.de.bruin@nlr.nl

References

[1] Tezok F, Ernest F. : Icing Tunnel Testing Methodology: Pre-Test CFD, Tunnel Peculiarities, Scaling effects, *Proceedings of The Aerodynamics Symposium*, Vol. 6, pp. 81-100, 1997.

[2] Papadakis M, Hung K, Vu G, Yeong H, Bidwell C, Breer M, Benice T : Experimental investigation of water droplet impingement on airfoils, finite wings and S-duct engine inlet, *NASA TM-2002-211700*, 2002.

[3] Ahn G, Jung K, Myong R, Shin H, Habashi W: Computational and experimental investigation of ice accretion on the surface of rotorcraft air intake anti-icing system, AIAA 2013-1077.

[4] Ferrigno F. IWT User manual, CIRA CF-04-0541 Rev1.

[5] Bellucci M, Esposito B, Marrazo M, Fatigati G, Ferrigno F: Calibration of CIRA IWT in the low speed configuration, AIAA 2007-1092.

ID #	LWC	MVD	Temp	Ts	Duration	Altitude (ISA)	AoA	AoS	Related Icing Condition
	(g/m^3)	(μm)	(K)	(°C)	(sec)	[m]	(deg)	(deg)	
3	0.60	20.0	263.1	-9.9	496	1500	-5	-2	DEF-CMI
6	0.99	20.0	278.0	5.0	496	1500	-5	-2	DEF-CMI
7	0.80	20.0	271.0	-2.0	496	1501	-5	-2	DEF-CMI
8	0.60	20.1	262.9	-10.1	496	1500	-5	-2	DEF-CMI
9	0.30	20.2	252.8	-20.2	496	1500	-5	-2	DEF-CMI
10	0.20	20.1	243.3	-29.7	512	1500	-5	-2	DEF-CMI
10-bis	0.20	20.2	242.8	-30.2	496	1500	-5	-2	DEF-CMI
11	1.00	20.1	266.9	-6.1	74	1500	-5	-2	DEF-IMI
12	0.91	20.2	262.6	-10.4	74	1499	-5	-2	DEF-IMI
13	0.46	20.4	252.7	-20.3	74	1500	-5	-2	DEF-IMI
14	0.31	20.4	243.2	-29.8	74	1500	-5	-2	DEF-IMI
15	0.60	19.9	263.0	-10.0	782	4300	-1	-1	DEF-CMI
16	0.21	20.2	243.1	-29.9	782	4300	-1	-1	DEF-CMI
17	0.91	20.0	263.3	-9.7	117	4301	-1	-1	DEF-IMI
18	0.31	20.1	243.0	-30.0	117	4301	-1	-1	DEF-IMI
19	0.31	20.2	272.0	-1.0	1800	-8	0	0	Ground Idle
20	0.73	39.7	272.0	-1.0	1800	-7	5	0	Hover IGE
21	0.20	20.2	243.1	-29.9	1200	4267 to 0	5	0	Flight Idle Descent
22	0.60	20.0	263.0	-10.0	1200	1500	-5	-2	heater off
23	**0.84**	**20.1**	270.9	**-2.1**	**1200**	**1500**	-5	-2	**DEF-CMI**
26	**1.10**	**40.2**	267.0	**-6.0**	**74**	**1503**	**-5**	**-2**	**DEF-IMI**
30	**0.67**	**30.0**	263.1	**-9.9**	**496**	**1500**	**-5**	**-2**	**DEF-CMI**
32	**0.59**	**20.0**	263.0	**-10.0**	**496**	**4300**	**-5**	**-2**	**DEF-CMI**
35	**0.60**	**20.0**	**263.0**	**-10.0**	**496**	**1500**	**-5**	**-2**	**DEF-CMI**

Table 1: Summery of test conditions for DEF-CMI and DEF-IMI anti-icing tests

Copyright Statement